

# Antisite defects in Ce-doped YAG ( $\text{Y}_3\text{Al}_5\text{O}_{12}$ ): First-principles study on structures and 4f-5d transitions

Ana Belén Muñoz-García,<sup>1</sup> Zoila Barandiarán,<sup>2,3</sup> and Luis Seijo<sup>2,3</sup>

<sup>1</sup>*Department of Chemical Sciences, University of Naples Federico II,*

*Via Cintia 21, 80126 Naples, Italy*

<sup>2</sup>*Departamento de Química, Universidad Autónoma de Madrid, 28049 Madrid, Spain*

<sup>3</sup>*Instituto Universitario de Ciencia de Materiales Nicolás Cabrera,*

*Universidad Autónoma de Madrid, 28049 Madrid, Spain*

(Dated: July 30, 2012)

## Abstract

The interactions between  $\text{Ce}^{3+}$  and antisite defects (AD) in YAG ( $\text{Y}_3\text{Al}_5\text{O}_{12}$ ) are studied by means of first-principles calculations: Periodic-boundary-conditions density-functional-theory for a 160 atom YAG unit cell with one  $\text{Ce}^{3+}$  and one or two ADs, and complete-active-space second-order perturbation theory for the  $4f^1$ ,  $5d^1$ , and  $6s^1$  electronic manifolds of the  $(\text{CeO}_8\text{Al}_2\text{O}_4)^{15-}$  embedded cluster. Attractive interactions are found between  $\text{Ce}^{3+}$  and the ADs. The formation of one AD is more favorable in Ce:YAG than in YAG, but the formation of a second AD is less favorable, which means that the presence of Ce tends to lower the concentration of antisite defects in YAG. The interaction between  $\text{Ce}^{3+}$  and antisite defects blueshifts the two lowest  $\text{Ce}^{3+}$   $4f \rightarrow 5d$  transitions. This result rules out the involvement of antisite defects in the recently reported excitation of the lowest  $5d \rightarrow 4f$  emission with photons below the zero-phonon line and leaves other distorted Cerium centers for consideration, like  $\text{Ce}^{3+}$  interacting with interstitial non-stoichiometric Yttrium or with vacancies. The reasons behind the blueshifts are analyzed in detail: They are dominated by a decrease in the effective ligand-field splitting of the  $5d^1$  manifold, almost entirely due to the structural changes of short- and long-range and with almost negligible electronic effects from the Y and Al site exchanges.

PACS numbers: 71.55.-i, 71.15.Dx, 61.72.-y, 61.72.jn, 61.72.S-, 78.40.-q, 71.70.-d

## I. INTRODUCTION

Yttrium aluminum garnet  $\text{Y}_3\text{Al}_5\text{O}_{12}$  (YAG) doped with  $\text{Ce}^{3+}$  (Ce:YAG) is a well known phosphor used in white solid-state-lighting (SSL) devices due to its ability to convert to yellow part of the blue light emitted by a GaN light-emitting-diode (LED)<sup>1-3</sup>. The blue absorption and yellow emission are due to  $4f \rightarrow 5d$  and  $5d \rightarrow 4f$  transitions of  $\text{Ce}^{3+}$  and they are known to depend on the local structure of the  $\text{Ce}_Y$  substitutional defect. For instance, changing the local structure of the active defects via co-doping has been used as a practical means to blue- and red-shift the  $5d \rightarrow 4f$  emission<sup>4-7</sup> in an attempt to control the color of the phosphor, an issue which is considered one of the keys for the success of SSL technologies.<sup>8</sup> Also, the lowest  $5d \rightarrow 4f$  emission has recently been excited with photons  $1650 \text{ cm}^{-1}$  below the zero-phonon line<sup>9</sup> and this phenomenon has been explained with the involvement of phonon-assisted nonradiative energy transfer between different groups of distorted  $\text{Ce}^{3+}$  centers, like the ones resulting from the interactions with antisites, interstitial non-stoichiometric Yttrium, or vacancies. And the interplay between  $\text{Ce}^{3+}$  ions and different defects is known to play important roles in the different optical behaviors of Ce:YAG in its different forms, like single-crystal, single-crystalline film, nanopowder, and transparent optical ceramics.<sup>9-12</sup> Hence, it is important to know the interactions between  $\text{Ce}^{3+}$  and other defects present in YAG, which could be formed intentionally (like co-dopants) or as a result of the preparation methods (like antisite defects, interstitials, or vacancies).

First-principles calculations have been able to model reasonably well the  $4f^1$  and  $5d^1$  manifolds of  $\text{Ce}^{3+}$  in YAG, both in its ideally isolated defect<sup>13</sup> and in the complex defects resulting from its interactions with co-dopants like  $\text{Ga}^{3+}$  [Ref. 14] and  $\text{La}^{3+}$  [Ref. 15]. In effect, in the case of the  $\text{Ce}_Y$  single substitutional defect, wave function based *ab initio* embedded-cluster calculations on the states of the  $4f^1$  and  $5d^1$  configurations (complete-active-space self-consistent-field<sup>16-18</sup> based second-order many-body perturbation theory<sup>19-22</sup> CASSCF/CASPT2) predicted its ground structure (later seen to agree reasonably well with EXAFS measurements<sup>23</sup>) and excited state structures, and computed its absorption and emission spectra, which helped solving remaining assignment issues<sup>24</sup>. In the cases of  $\text{Ga}^{3+}$  and  $\text{La}^{3+}$  co-doped Ce:YAG, combined periodic-boundary-conditions density-functional-theory<sup>25,26</sup> (DFT) calculations and embedded-cluster CASSCF/CASPT2 calculations reproduced the opposite shifts experienced with both co-dopings<sup>14,15</sup> (blueshift with  $\text{Ga}^{3+}$  and

redshift with  $\text{La}^{3+}$ ) and answered the long standing question of why they are opposite if both co-dopings induce lattice expansions<sup>27,28</sup>: The  $\text{Ga}_{\text{Al}}$  defect does not have a preference to sit near Ce and its effects are dominated by the reduction of the ligand field splitting of the  $5d$  shell due to the structural expansion, resulting in a blueshift of the lowest  $4f - 5d$  transition. On the contrary,  $\text{La}_{\text{Y}}$  tends to be located in sites close to Ce, which results in a reduction of the difference between  $4f$  and  $5d$  energy centroids and in a stronger Pauli repulsion between Ce and La (with respect to the smaller Y) that produces a relevant increase of the effective ligand field; both effects together compensate the consequences of the lattice expansion and lead to the final redshift.

In this paper, we use the above first-principles methods in order to study the interplay between the  $\text{Ce}_{\text{Y}}$  defect and  $\text{Y}_{\text{Al}}\text{-Al}_{\text{Y}}$  antisite defects (AD) in YAG, which are dominant among the intrinsic defects<sup>29,30</sup>. In single crystal form, these ADs, in which Y and Al exchange sites, lower the real symmetry of the pure garnet from cubic to trigonal<sup>29</sup>. They are known to be present in all forms of YAG and their concentrations are strongly dependent on the preparation method, mostly on the temperature<sup>9-12</sup>. Here, we focus on the interactions between  $\text{Ce}^{3+}$  and the ADs and on how they impact their structures and the  $4f^1$  and  $5d^1$  energy manifolds of  $\text{Ce}^{3+}$  in YAG. The possibility of involvement of ADs in the excitation of the  $5d - 4f$  luminescence below the zero-phonon line observed by Feofilov *et al.*<sup>9</sup> is discussed.

In order to address the study, we take advantage of previous DFT calculations that provided a detailed picture of the local atomistic structures, the electronic structure, and the distribution of ADs within the pure YAG host<sup>31</sup> and we carry out a first-principles combined theoretical study of YAG with Ce and antisite defects together,  $\text{Ce,AD:YAG}$ . Firstly, we perform ground state periodic-boundary-conditions DFT calculations of the atomistic structures of  $\text{Ce,AD:YAG}$ , with concentrations of one  $\text{Ce}_{\text{Y}}$  impurity and one or two ADs per unit cell. Then, the computed structures are used in CASSCF/CASPT2 calculations performed on the ground and excited states of the  $(\text{CeO}_8\text{Al}_2\text{O}_4)^{15-}$  cluster under the effects of embedding potentials of YAG with antisite defects. Out of these, the energies of the  $4f - 5d$  transitions of  $\text{Ce}^{3+}$  are calculated under the effect of one and two antisite defects.

The details of the calculations are presented in Sec. II, the results are discussed and analyzed in Sec. III, and the conclusions are presented in Sec. IV.

## II. DETAILS OF THE CALCULATIONS

The atomistic structures of  $\text{Y}_{2.875}\text{Ce}_{0.125}\text{Al}_5\text{O}_{12}$  materials containing one and two anti-site defects per unit cell (Ce,1AD:YAG and Ce,2AD:YAG respectively) have been obtained with the periodic boundary conditions self-consistent SIESTA method,<sup>32,33</sup> using density functional theory (DFT)<sup>25,26</sup> within the generalized gradient approximation (GGA) as formulated by Perdew, Burke, and Ernzerhof (PBE).<sup>34,35</sup> We used norm-conserving pseudopotentials<sup>36</sup> in the Kleinman-Bylander form.<sup>37</sup> For Y, Al, and O, we used those generated for and used in pure YAG,<sup>38</sup> and for Ce we used its relativistic version<sup>39</sup> for the reference configuration  $\text{Ce}^{3+}(5s^24p^64f^1)$ , previously used in Ce,La and Ce,Ga co-doped YAG.<sup>14,15</sup> Nonlinear partial-core corrections<sup>40</sup> and semicore states to account for large core-valence overlap have been used for Y and Ce. Atomic basis sets of double- $\zeta$  plus polarization quality have been used for all atoms: Y( $5s5s'4p4p'5p4d4d'$ ), Al( $3s3s'3p3p'3d$ ), O( $2s2s'2p2p'3d$ ), and Ce( $5s6s6s'5p5p'6p5d5d'4f$ ). The basis sets of Y, Al, and O have been generated in Ref. 38 and that of Ce in Ref. 15, all of them using the fictitious enthalpy method of Anglada *et al.*<sup>41</sup> The charge density has been projected on a uniform grid in real space, with an equivalent plane-wave cutoff of 380 Ry, in order to calculate the exchange-correlation and Hartree matrix elements. Total energy calculations have been converged with respect to  $k$ -space integration; a  $k$  grid cutoff of 15.0 Bohr was used.

All geometry optimizations have been performed without imposing any symmetry restrictions in the positions of all atoms in the 160 atom unit cell, using a conjugate gradient method, with a force tolerance of 0.04 eV/Å. Starting geometries were generated from the computed atomistic structure of perfect YAG ( $a=12.114$  Å,  $x(\text{O})=-0.036$ ,  $y(\text{O})=0.0519$  and  $z(\text{O})=0.1491$ ),<sup>38</sup> in good agreement with experiment,<sup>42</sup> after generating the  $\text{Ce}_Y$  and AD defects by substituting Y atoms by Ce and exchanging Y and Al positions. In preliminary calculations, we have explored the change in volume experimented by the unit cell of YAG containing  $\text{Ce}_Y$  and one or two ADs by allowing the cell to breath after optimization of each set of defects. The increments in the lattice constant found are +0.17% and +0.44% for Ce,1AD:YAG and Ce,2AD:YAG respectively. We consider them small enough to neglect the lattice expansion effects on the defect structures.

The optical absorption energies corresponding to the  $\text{Ce}^{3+} 4f \rightarrow 4f$ ,  $4f \rightarrow 5d$ , and  $4f \rightarrow 6s$  transitions in Ce,1AD:YAG and Ce,2AD:YAG have been calculated with embedded

cluster wave function based methods. For this purpose, the  $(\text{CeO}_8\text{Al}_2\text{O}_4)^{15-}$  cluster was embedded in *ab initio* model potential (AIMP)<sup>43</sup> representations of the corresponding hosts, with their structures distorted by the presence of the defects. The cluster is made of the Cerium ion and its first oxygen coordination shell  $\text{CeO}_8$ , plus two additional  $\text{AlO}_2$  atomic sets so as to include the two  $\text{AlO}_4$  moieties that share two oxygens each with the  $\text{CeO}_8$  unit (Fig. 1). This choice is made on the basis of previous investigations that pointed out the presence of strongly bound  $-\text{Y}-\text{AlO}_4-\text{Y}-\text{AlO}_4-$  chains in YAG.<sup>44</sup> The AIMP embedding potentials of the  $\text{Y}^{3+}$ ,  $\text{Al}^{3+}$ , and  $\text{O}^{2-}$  ions in YAG, which include electrostatic, exchange, and Pauli repulsion interactions between the cluster and its environment, were produced in Ref. 15 according to the prescriptions in Ref. 45. They were located at the atomic positions that resulted from the PBC-DFT calculations of the previous step.

A relativistic effective core potential ([Kr] core) and a  $(14s10p10d8f3g)/[6s5p6d4f1g]$  Gaussian valence basis set from Ref. 46 was used for Ce. For O, a [He] effective core potential and a  $(5s6p1d)/[3s4p1d]$  valence basis set from Ref. 47 was used, extended with one p-type diffuse function for anion<sup>48</sup> and one d-type polarisation function<sup>49</sup>. For Al, we used a [Ne] core potential and a  $(7s6p1d)/[2s3p1d]$  valence basis set from Ref. 47, which includes one d-type polarisation function.<sup>49</sup> Extra basis set functions were added in order to improve the degree of orthogonality achieved between the cluster molecular orbitals and the environmental orbitals: the  $\text{Y}^{3+}$   $3d, 4s, 4p$  and the  $\text{Al}^{3+}$   $2s, 2p$  atomic orbitals of all Y and Al next to the cluster in Ce:YAG, as obtained in self-consistent embedded-ions calculations on YAG,<sup>13</sup>. These embedding potentials, effective core potentials, and basis sets have previously been used in first-principles simulations of Ce:YAG absorption and luminescence<sup>13</sup> and they are available from the authors<sup>50</sup>.

In the  $(\text{CeO}_8\text{Al}_2\text{O}_4)^{15-}$  embedded cluster, spin-orbit free relativistic calculations have been performed using the atomistic structures resulting from the ground state periodic DFT calculations described above. Bonding, static and dynamic correlation, and scalar relativistic effects are taken into account in state-average complete active space self consistent field (SA-CASSCF)<sup>16–18</sup> plus multistate second-order perturbation theory (MS-CASPT2)<sup>19–22</sup> calculations performed with a scalar relativistic many-electron Hamiltonian. Spin-orbit coupling effects are missing in these calculations, but their effect on the  $4f \rightarrow 5d$  transitions of Ce:YAG, which are the focus of this paper, are known to be a uniform increment of around  $1000 \text{ cm}^{-1}$  with negligible dependence on the atomistic structure<sup>13</sup>.

In the SA-CASSCF calculations, a  $[4f, 5d, 6s]^1$  CAS was used, meaning that the wave functions are configuration interaction (CI) wave functions that mix all configurations with one unpaired electron occupying one of the thirteen molecular orbitals of main character Ce-4*f*, Ce-5*d*, and Ce-6*s*. The molecular orbitals are chosen so as to minimize the average energy of the thirteen states. As a consequence of the presence of the antisite defects, the local  $D_2$  symmetry of the Ce site in Ce:YAG is lost and the thirteen states belong to the only irreducible representation of the point group  $C_1$  used in our calculations. They are classified as  $1 - 13^2A$ , although the relative energies of the  $4f^1$ ,  $5d^1$ , and  $6s^1$  configurations are maintained, as we will see later, and  $1 - 7^2A$  are basically of Ce-4*f*<sup>1</sup> character,  $8 - 12^2A$  are basically of Ce-5*d*<sup>1</sup> character, and  $13^2A$  of Ce-6*s*<sup>1</sup> character.

Using the CASSCF wave functions and the occupied and virtual molecular orbitals, MS-CASPT2 calculations are done where the dynamic correlation effects (which are missing at the CASSCF level) of the 5*s*, 5*p*, 4*f* and 5*d* electrons of Cerium and the 2*s* and 2*p* electrons of the eight Oxygen atoms are added. These calculations have been performed with the program MOLCAS<sup>51</sup>.

### III. RESULTS AND DISCUSSION

#### A. Structure and energetics

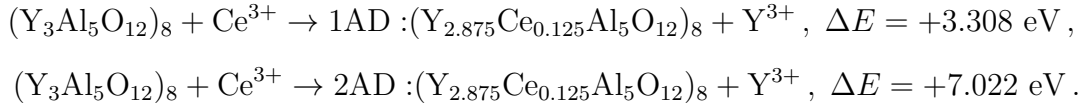
We have studied YAG unit cells containing one Ce<sub>Y</sub> defect together with one and two antisite defects per unit cell. In order to investigate and choose among all possible combinations, we resorted to the structural information obtained in previous first-principles studies on pure YAG with one and two ADs per unit cell.<sup>31</sup> In the Ce,1AD:YAG case, the 23 non-equivalent positions of Ce<sub>Y</sub> coupled with the most stable single AD are indicated in the upper part of Fig. 2. In the Ce,2AD:YAG case, there are 11 non-equivalent positions of Ce<sub>Y</sub> coupled with the most stable double AD; they are indicated in the lower part of Fig. 2. The relative energies of all the Ce,1AD and Ce,2AD multiple defects studied are shown in Tables I and II, respectively, together with summaries of the structural data: off-center displacements of Ce<sub>Y</sub>, Y<sub>Al</sub>, and Al<sub>Y</sub> with respect to their respective substituted ions in YAG and inter-cation distances in YAG, Ce:YAG, Ce,1AD:YAG, and Ce,2AD:YAG, indicative of the mutual effects of Ce<sub>Y</sub> and the ADs.

Among all the Ce,1AD:YAG defects studied, we have not found any pattern relating defect energies and off-center displacements of inter-cation distances. One of them (defect 1a) is significantly more stable than the others and it is not characterized by any special features, neither of the cationic off-center displacements nor of the Ce-AD distances. It has low off-center displacements of  $\text{Ce}_Y$  with respect to YAG and of  $\text{Y}_{\text{Al}}$  and  $\text{Al}_Y$  with respect to 1AD:YAG, but it is not the defect with the lowest ones. It isn't either the defect with shortest nor longest  $\text{Ce}_Y\text{-Y}_{\text{Al}}$  and  $\text{Ce}_Y\text{-Al}_Y$  distances. We comment below the specific structural features of defect 1a. In the Ce,2AD:YAG case, there is also one defect more stable than the others (defect 2k), although not as singled out as in the 1AD case, followed by a few with similar energies, and there is one significantly more unstable than the rest (defect 2a), which is the one that shows the largest  $\text{Ce}_Y$  off-center displacement and the strongest distortion of the  $\text{Ce}_Y\text{-Al}_{\text{oct}}$  distance.

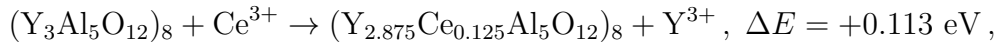
Let us now analyze the local structure of most stable Ce,1AD:YAG and Ce,2AD:YAG defects (defects 1a and 2k, respectively, in Fig.2). In both cases,  $\text{Ce}^{3+}$  originally substitutes for  $\text{Y}^{3+}$  on a  $D_2$  point symmetry site, with four shorter and four larger Ce-O distances, labeled s1-s4 and l1-l4 in Figs. 3 and 4. The local structure of the Ce,1AD:YAG defect 1a is shown in Fig. 3. The  $\text{Ce}_Y$  and  $\text{Al}_Y\text{-Y}_{\text{Al}}$  defects are linked by a  $\text{AlO}_4$  moiety that connects the  $\text{Ce}_Y\text{O}_8$  unit, via two short Ce-O bonds (s1 and s2), with the  $\text{Al}_Y\text{O}_8$  unit of the AD. They form a  $\dots\text{-Ce}_Y\text{-AlO}_4\text{-Al}_Y\text{-AlO}_4\text{-Ce}_Y\text{-}\dots$  chain, in which all the Y atoms of the original  $\dots\text{-Y-AlO}_4\text{-Y-AlO}_4\text{-Y-}\dots$  chain of YAG (Ref. 44) are alternatively substituted by Ce and Al. The presence of the  $\text{Y}_{\text{Al}}$  in the ADs slightly distorts the symmetry of the original chain, as it is shown by the  $\text{Ce}_Y\text{-Al}_Y$  distances (6.083 and 6.089 Å, very slightly longer for the AD with closest  $\text{Ce}_Y\text{-Y}_{\text{Al}}$ ) and the  $\text{Al}_Y\text{-Ce}_Y\text{-Al}_Y$  angle (169°, 11° smaller than the original Y-Y-Y angle of 180°). The mutual distortions between Ce and the AD are illustrated in Table III.  $D_2$  point symmetry disappears around Ce and its coordination shell experiences an overall expansion (of 0.038 Å in average) in which both short and long Ce-O bonds are affected in a similar way. The effect of Ce on the AD structure is important only on the  $\text{Al}_Y$  in the  $\dots\text{-Ce}_Y\text{-AlO}_4\text{-Al}_Y\text{-AlO}_4\text{-Ce}_Y\text{-}\dots$  chain and insignificant on the  $\text{Y}_{\text{Al}}$  off chain. The distortion around  $\text{Al}_Y$  maintains its quasi-sixfold coordination of 1AD:YAG (Ref. 31) with six short  $\text{Al}_Y\text{-O}$  distances and two much longer ones; three of the closer Oxygen atoms move significantly inwards (d3, d4, b2) and one moves outwards (d5); the two more distant Oxygen atoms (d1, b1) suffer slight displacements (shortening and elongation respectively).

The local structure of the most stable Ce<sub>2</sub>AD:YAG defect (2k) is shown in Fig. 4. Here, Ce<sub>Y</sub> is directly linked to one of the two antisites of the 2AD defect. In this case two Oxygen atoms of the Ce<sub>Y</sub>O<sub>8</sub> unit (one with short and one with long Ce-O distances, s1 and l1) are shared with one of the Y<sub>Al</sub>O<sub>6</sub> units of the 2AD. The mutual distortions between Ce and the 2AD are illustrated in Table IV. As in the 1AD case,  $D_2$  point symmetry disappears around Ce and its coordination shell experiences an overall expansion; this is slightly larger than in the 1AD case (of 0.041 Å in average) and more anisotropic, slightly stronger for the long than for the short Ce-O bonds (+0.044 vs. +0.038 Å). The two Oxygen atoms linked to the 2AD (s1 and l1) are the ones that experience the smaller rearrangements; the O<sub>s1</sub>-Ce<sub>Y</sub>-O<sub>l1</sub> angle opens slightly from 73.5° in Ce:YAG to 76.2° in Ce<sub>2</sub>AD:YAG. The structure of the double AD defect remains very much unaffected by the presence of Ce<sub>Y</sub>; the Y<sub>Al</sub>O<sub>6</sub> unit linked to Ce<sub>Y</sub>O<sub>8</sub> suffers very small changes and propagates the very small distortion to the next Al<sub>Y</sub>O<sub>8</sub> unit, the only significant change being the lower distance between Al<sub>Y</sub> and one of its two loose Oxygen atoms (d1).

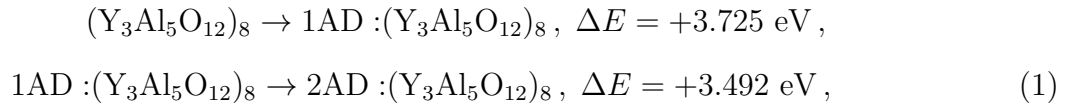
The formation energies of the most stable Ce<sub>1</sub>AD:YAG and Ce<sub>2</sub>AD:YAG defects (1a and 2k, respectively), taking the Ce<sup>3+</sup> and Y<sup>3+</sup> free ions as a reference, are the following:



These, together with the corresponding formation energies of one Ce<sub>Y</sub> defect,<sup>14</sup>



and of one and two Al<sub>Y</sub>-Y<sub>Al</sub> antisite defects,<sup>31</sup>

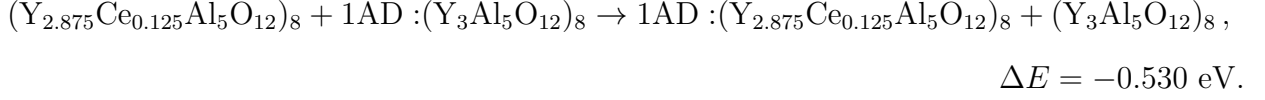


allows us to complete Fig. 5, where the formation energies of single and multiple defects are summarized.

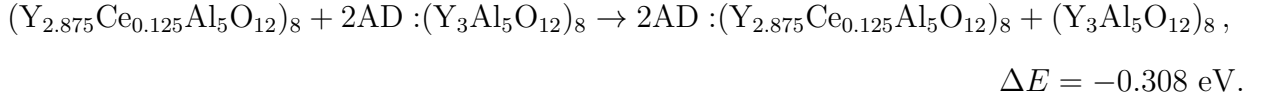
We can observe that the formation of one Ce<sub>Y</sub> defect is 0.530 eV (51.1 kJ/mol) more favorable in YAG with one antisite defect per unit cell (−0.417 eV) than in perfect YAG (+0.113 eV). Equivalently, the formation of one Al<sub>Y</sub>-Y<sub>Al</sub> antisite defect is also 0.530 eV more favorable in Ce-doped YAG with one Ce<sub>Y</sub> defect per unit cell (+3.195 eV) than in



perfect YAG (+3.725 eV). So, -0.530 eV is just the interaction energy between the  $\text{Ce}_Y$  and  $\text{Al}_Y\text{-Y}_{\text{Al}}$  individual defects,



Also from Fig. 5, it can be seen that the formation energy of a  $\text{Ce}_Y$  defect is more favorable in YAG containing two antisite defects (-0.195 eV) than in perfect YAG (+0.113 eV). Analogously, this favorable difference in energy (0.308 eV) is also found in the process of formation of two antisite defects from Ce:YAG (+6.909 eV) with respect to the formation of two antisite defects from pure YAG (+7.217 eV). Thus, -0.308 eV is the energy accounting for the interaction between the  $\text{Ce}_Y$  impurity and the defect formed by the two pairs of  $\text{Y}_{\text{Al}}$  and  $\text{Al}_Y$  :



In the favorable interaction between  $\text{Ce}_Y$  and the ADs, relaxation cooperative factors play a important role: 0.307 eV in Ce,1AD:YAG and 0.200 eV in Ce,2AD:YAG. (In Ce,1AD:YAG, the stress energy from the perfect YAG structure is 6.612 eV and the sum of the separated relaxation energies of  $\text{Ce}_Y$  in Ce:YAG<sup>44</sup> and of 1AD in 1AD:YAG<sup>31</sup> is 6.305 eV. In Ce,2AD:YAG, relaxation of the whole structure stabilizes the energy by 12.965 eV and the sum of the separated relaxation energies of  $\text{Ce}_Y$  in Ce:YAG<sup>44</sup> and of 2AD in 2AD:YAG<sup>31</sup> is 12.765 eV.)

The above results show that, whereas making the first AD is 0.530 eV more favorable in Ce:YAG than in YAG, creating the second AD demands 0.222 eV more in Ce,1AD:YAG than in 1AD:YAG, 0.107 eV of them due to the stress associated with its more difficult accommodation when  $\text{Ce}_Y$  is present. Then, the presence of Ce impurities at the concentrations studied in this work changes the pattern of antisite defects present in pure YAG in favor of the formation of one antisite defect per YAG unit cell, instead of the two antisite defects per unit cell obtained for YAG in the absence of Ce-doping<sup>31</sup> (which was in agreement with experiments<sup>29</sup>). In other words, Ce tends to lower the AD concentration in YAG. This result is in line with the observations of Pankratov *et al.* in Ce-doped YAG nanocrystals<sup>11</sup>.

## B. Electronic structure

Calculated total and projected densities of states (DOS and PDOS) of the Ce,1AD:YAG and Ce,2AD:YAG materials with their most stable defective structures (defects 1a and 2k, respectively) are shown in Figs. 6 and 7, with zero energy taken as the top of the valence band of AD-free YAG, which has oxygen  $2p$  character.<sup>38</sup> Their Ce-related features are very similar to those of Ce:YAG (Ref. 44) and the AD-related features very similar to those of 1AD:YAG and 2AD:YAG (Ref. 31):  $\text{Ce}_Y$  introduces new  $5p$  occupied states between -18 and -16 eV and between -14 and -12 eV not present in pure YAG; occupied  $4f$  states of the impurity appear above the top of the YAG valence band and empty states of Ce  $4f$ ,  $5d$  and  $6s$  character appear below the bottom of the conduction band; the upper occupied levels of the two Oxygen atoms of the ADs that can be considered unbound to  $\text{Al}_Y$  (Oxygen atoms d1 and b1 in Tables III and IV)<sup>31</sup> rise in energy with respect to 1AD:YAG and 2AD:YAG, but they still lie below Ce  $4f$  levels in Ce,1AD:YAG and Ce,2AD:YAG. In Fig. 8 we show in detail the PDOS of the Ce  $4f$   $\alpha$  states in the gap of Ce:YAG, Ce,1AD:YAG, and Ce,2AD:YAG. Small shifts to lower energies with respect to Ce:YAG are observed in the occupied states (0.30 eV in Ce,1AD:YAG and 0.45 eV in Ce,2AD:YAG). Equal shifts are experienced in these materials by the inner Ce  $5s$  and  $5p$  levels, which indicates that they are not due to changes in the bonding between Ce- $4f$  and O- $2p$ , but to the change in the electrostatic field on Ce created by the anisotropic distortions of its environment produced by the ADs. The shifts of the lowest lying unoccupied states to lower energies are larger (0.80 eV in Ce,1AD:YAG and 0.50 eV in Ce,2AD:YAG).

## C. Electronic transitions

The energies of the Ce- $4f^1$ , Ce- $5d^1$ , and Ce- $6s^1$  levels of Ce:YAG, Ce,1AD:YAG and Ce,2AD:YAG, relative to their respective ground states, as obtained in CASPT2 calculations on the  $(\text{CeO}_8\text{Al}_2\text{O}_4)^{15-}$  cluster under the effects of the embedding potentials of each material, are shown in Table V. The atomic positions of the cluster atoms and of the embedding atoms have been taken from the previously discussed PBC-DFT calculations. The energies so calculated are vertical (Frank-Condon) transitions and they correspond to the maxima of the experimental absorption bands.<sup>27</sup> Successful comparisons of the theoretical absorption

transitions of Ce:YAG with experiments have been done elsewhere<sup>13,15</sup> and here we will focus on the effects of the ADs. The shifts induced in the transitions by the presence of one and two ADs per unit cell are also included in the Table. In the calculations, the shifts come from the distortions of the atomic coordinates of  $(\text{CeO}_8\text{Al}_2\text{O}_4)^{15-}$ , the distortions of the atomic coordinates of the rest of the atoms of the materials, and the electronic effects due to  $\text{Y}_{\text{Al}}$  and  $\text{Al}_{\text{Y}}$  substitutions. According to these calculations, the antisite defects of YAG alter the  $4f \rightarrow 4f$  transitions of  $\text{Ce}^{3+}$  in amounts that are small in absolute terms although significant in percentage. They slightly blueshift the two lowest  $4f \rightarrow 5d$  transitions.

In order to contrast this result with experiments, we can say that Pankratov *et al.*<sup>11</sup> report that the second  $4f - 5d$  transition is shifted to the lower energy side from Ce-doped YAG single crystals to Ce-doped YAG nanocrystals, where the concentration of ADs is significantly lower. This would be in agreement with the present findings. Even if the existence of surface defects in nanocrystals could be playing a role here, the present calculations indicate that the lower concentration of ADs cannot be ruled out as responsible for this redshift. Regarding the first  $4f - 5d$  transition, we aren't aware of specific reports on its experimental shift by the interaction of Ce with ADs; however, the data in Fig. 4 of Ref. 10 on the luminescence spectra of Ce-doped YAG single crystals and single crystalline films (with lower AD concentration in the latter case) seem to indicate that it experiences a small blueshift when the AD concentration is higher. This would also be in agreement with the present calculations.

The blueshift of the first  $\text{Ce}^{3+}$   $4f - 5d$  transition by the interaction with ADs rules out the involvement of antisite defects in the excitation of the lowest  $5d \rightarrow 4f$  emission with photons  $1650 \text{ cm}^{-1}$  below the zero-phonon line observed by Feofilov *et al.*,<sup>9</sup> which was one of the possibilities considered to explain this phenomenon. This leaves the other distorted  $\text{Ce}^{3+}$  centers suggested by the authors for consideration ( $\text{Ce}^{3+}$  interacting with interstitial non-stoichiometric Yttrium or with vacancies).

The reasons behind the blueshift of the lowest  $4f \rightarrow 5d$  transitions can be analyzed following the procedure described in Ref. 15. In short, following the diagram in Fig. 9, the energy of, e.g., the lowest  $4f \rightarrow 5d$  transition can be decomposed in terms of a centroid contribution and a ligand-field contribution,

$$\Delta E(1 - 4f^1 \rightarrow 1 - 5d^1) = \Delta E_{\text{centroid}}(4f^1 \rightarrow 5d^1) + \Delta E_{\text{ligand-field}}(1 - 4f^1 \rightarrow 1 - 5d^1), \quad (2)$$

with

$$\Delta E_{\text{centroid}}(4f^1 \rightarrow 5d^1) = \frac{1}{5} \sum_{i=1,5} E(i - 5d^1) - \frac{1}{7} \sum_{i=1,7} E(i - 4f^1), \quad (3)$$

$$\Delta E_{\text{ligand-field}}(1 - 4f^1 \rightarrow 1 - 5d^1) = \Delta E_{\text{LF}}(1 - 4f^1) - \Delta E_{\text{LF}}(1 - 5d^1), \quad (4)$$

$$\Delta E_{\text{LF}}(1 - 4f^1) = \frac{1}{7} \sum_{i=1,7} E(i - 4f^1) - E(1 - 4f^1), \quad (5)$$

$$\Delta E_{\text{LF}}(1 - 5d^1) = \frac{1}{5} \sum_{i=1,5} E(i - 5d^1) - E(1 - 5d^1). \quad (6)$$

Also, comparing the results of a series of calculations prepared with adequate choices of atomic coordinates of the  $(\text{CeO}_8\text{Al}_2\text{O}_4)^{15-}$  cluster and its environment and of the embedding potentials, it is possible to extract the effects of the distortions of the first coordination shell around  $\text{Ce}_Y$ , the distortions of the rest of the solid, and the electronic effects due to the substitutions of Y by Al and Al by Y in the ADs.<sup>15</sup> The designs and the results of the mentioned calculations are shown in Table VI. In it, the A-B-C-D series of Ce,1AD:YAG and of Ce,2AD:YAG give: (1) the effects of the distortion of the first coordination shell of Ce (from A to B), (2) the effects of the distortion of the rest of the lattice (from B to C), and (3) the electronic effects brought about the exchange of Y and Al positions in the antisite defects (from C to D)). The analyses of Ce,1AD:YAG and Ce,2AD:YAG are summarized in Table VII.

In Ce,1AD:YAG, the last column of Table VII shows that the blueshift of the first  $4f \rightarrow 5d$  transition ( $461 \text{ cm}^{-1}$ ) is dominated by the ligand-field contribution ( $502 \text{ cm}^{-1}$ ), which is slightly corrected by the shift of the  $4f^1$  and  $5d^1$  centroids ( $-41 \text{ cm}^{-1}$ ). The ligand-field contribution comes entirely from the reduction of the ligand-field splitting of the  $5d^1$  manifold. Roughly speaking, the expansion of the first coordination shell of Ce accounts for two thirds of it; the structural rearrangements further away from it account for the other third. The electronic effects of the mutual substitution of Y and Al are insignificant, as corresponds with the long Ce-Y and Ce-Al distances. The small redshift contribution of the energy centroids is due to compensations between structural effects on the first shell and on the rest of the host; the first shell alone would give  $-116 \text{ cm}^{-1}$  redshift.

In Ce,2AD:YAG, the higher blueshift of the first  $4f \rightarrow 5d$  transition ( $792 \text{ cm}^{-1}$ ) is also dominated by a larger ligand-field effect contribution ( $1084 \text{ cm}^{-1}$ ) counterpoised by

a stronger redshift contribution from the centroids ( $-292 \text{ cm}^{-1}$ ). As in Ce,1AD:YAG, the ligand-field contribution comes basically from the reduction of the ligand-field splitting of the  $5d^1$  manifold, which is due in equal parts to the expansion of the first-shell and the rearrangements in second and further shells. The Y and Al electronic effects slightly increase the effective  $5d$  ligand-field splitting (a larger Y substitutes for a smaller Al at a relatively small cation-Ce distance -see Fig. 4-, which slightly increments the Pauli repulsion experienced by Ce), so giving a small redshift contribution. The redshift contribution of the energy centroids is mostly due to the expansion of the first shell ( $-223 \text{ cm}^{-1}$ ), which is enhanced by Y and Al electronic effects ( $-81 \text{ cm}^{-1}$ ). In overall, the electronic effects brought about by the exchange of Y and Al sites is significantly larger in Ce,2AD:YAG than in Ce,1AD:YAG, which goes together with the shortest Ce-Y distance in the former.

Let us finally remark that the  $4f - 5d$  energy centroid,  $\Delta E_{\text{centroid}}(4f^1 \rightarrow 5d^1)$ , is lowered by the presence of antisite defects in spite of the fact that they induce ligand expansions around Ce. The usual simple model for this quantity (the only one presently available to the best of our knowledge), which is due to Judd and Morrison,<sup>52,53</sup> was successfully used by Dorenbos for the rationalization of  $4f - 5d$  centroids of lanthanide ions in many hosts,<sup>54</sup> and analyzed and refreshed by Bettinelly and Mocorgé,<sup>55</sup> predicts the  $4f - 5d$  energy centroid to increase with the distance between Ce and the ligands. This disagreement between the predictions of Judd-Morrison model and *ab initio* calculations for small changes of the Ce-ligand distances confirms previous observations of the same fact<sup>14,15,56</sup> and supports the conclusion that using the model for the prediction of small centroid shifts associated with small and/or anisotropic ligand distortions around lanthanides can be misleading.

#### IV. CONCLUSIONS

A mixed first-principles study has been conducted on the interactions between  $\text{Ce}_Y$  substitutional defects and  $\text{Y}_{\text{Al}}\text{-Al}_Y$  antisite defects in YAG. The study includes ground state structural periodic-boundary-conditions DFT calculations on YAG with one  $\text{Ce}_Y$  and one or two  $\text{Y}_{\text{Al}}\text{-Al}_Y$  antisite defects together per unit cell (Ce,1AD:YAG and Ce,2AD:YAG), and CASPT2 calculations on the  $4f^1$ ,  $5d^1$ , and  $6s^1$  electronic manifolds of the  $(\text{CeO}_8\text{Al}_2\text{O}_4)^{15-}$  cluster embedded in AIMP representations of the above defective structures of YAG.

The calculations show attractive interactions between  $\text{Ce}_Y$  and the antisite defects. The

presence of ADs, which are intrinsic in YAG, causes a strongly anisotropic expansion of the atomistic structure around the  $\text{Ce}_Y$  impurities as well as a strong distortion of much of the YAG unit cell. Whereas the formation of a first AD is more favorable in Ce:YAG than in YAG, the formation of the second AD is less favorable; in consequence, the presence of Ce tends to lower the concentration of antisite defects in YAG, which seems to be in agreement with experiments in Ce-doped YAG nanocrystals.

The interaction between  $\text{Ce}^{3+}$  and antisite defects blueshifts the two lowest  $\text{Ce}^{3+} 4f \rightarrow 5d$  transitions. This result rules out the involvement of antisite defects in the excitation of the lowest  $5d \rightarrow 4f$  emission with photons  $1650 \text{ cm}^{-1}$  below the zero-phonon line observed by Feofilov *et al.*,<sup>9</sup> which was one of the possibilities considered to explain this phenomenon, and leaves the other distorted  $\text{Ce}^{3+}$  centers suggested by the authors for consideration ( $\text{Ce}^{3+}$  interacting with interstitial non-stoichiometric Yttrium or with vacancies).

The blueshifts are dominated by a decrease in the effective ligand-field splitting of the  $5d^1$  manifold, which is almost entirely due to the structural changes with almost negligible electronic effects from the  $\text{Y}_{\text{Al}}\text{-Al}_Y$  site exchange. Not only the expansion of the first coordination shell around  $\text{Ce}_Y$  is important for the reduction of the  $5d$  ligand-field, but also the distortions further away. The AD effects on the difference between the  $5d^1$  and  $4f^1$  energy centroids have a minor importance. Interestingly, the expansions around  $\text{Ce}_Y$  are accompanied by a lowering of the  $4f - 5d$  centroid difference; this is not anticipated by the usual model for this quantity, which predicts the opposite.

## Acknowledgments

This work was partly supported by grants from Ministerio de Economía y Competitividad, Spain (MAT2008-05379/MAT and MAT2011-24586).

---

<sup>1</sup> J. Y. Tsao, IEEE Circuits & Devices **20**, 28 (2004).

<sup>2</sup> S. Nakamura and G. Fasol, *The blue laser diode: GaN based light emitters and lasers* (Springer, Berlin, 1997).

<sup>3</sup> P. Schlotter, R. Schmidt, and J. Schneider, Appl. Phys. A **64**, 417 (1997).

<sup>4</sup> Y. Pan, M. Wu, and Q. Su, J. Phys. Chem. Solids **65**, 845 (2004).

- <sup>5</sup> Y. S. Lin, R. S. Liu, and B.-M. Cheng, *J. Electrochem. Soc.* **152**, J41 (2005).
- <sup>6</sup> H. S. Jang, W. B. Im, D. C. Lee, D. Y. Jeon, and S. S. Kim, *J. Lumin.* **126**, 371 (2007).
- <sup>7</sup> Y. X. Pan, W. Wang, G. K. Liu, S. Skanthakumar, R. A. Rosenberg, X. Z. Guo, and K. K. Li, *J. Alloys Compd.* **488**, 638 (2009).
- <sup>8</sup> J. Brodrick, *J. Disp. Technol.* **3**, 91 (2007).
- <sup>9</sup> S. P. Feofilov, et al., *J. Lumin.* (2012), <http://dx.doi.org/10.1016/j.jlumin.2012.06.030>.
- <sup>10</sup> Y. Zorenko, V. Gorbenko, I. Konstankevych, A. Voloshinovskii, G. Stryganyuk, V. Mikhailin, V. Kolobanov, and D. Spassky, *J. Lumin.* **114**, 85 (2005).
- <sup>11</sup> V. Pankratov, L. Grigorjeva, D. Millers, and T. Chudoba, *Radiat. Meas.* **42**, 679 (2007).
- <sup>12</sup> Y. Zorenko, T. Zorenko, V. V. Gorbenko, T. Voznyak, V. Savchyn, P. Bilski, and A. Twardak, *Opt. Mater.* **34**, 1314 (2012).
- <sup>13</sup> J. Gracia, L. Seijo, Z. Barandiarán, D. Curulla, H. Niemansverdriet, and W. van Gennip, *J. Lumin.* **128**, 1248 (2008).
- <sup>14</sup> A. B. Muñoz-García, J. L. Pascual, Z. Barandiarán, and L. Seijo, *Phys. Rev. B* **82**, 064114 (2010).
- <sup>15</sup> A. B. Muñoz-García and L. Seijo, *Phys. Rev. B* **82**, 184118 (2010).
- <sup>16</sup> B. O. Roos, P. R. Taylor, and P. E. M. Siegbahn, *Chem. Phys.* **48**, 157 (1980).
- <sup>17</sup> P. E. M. Siegbahn, A. Heiberg, B. O. Roos, and B. Levy, *Phys. Scr.* **21**, 323 (1980).
- <sup>18</sup> P. E. M. Siegbahn, A. Heiberg, J. Almlöf, and B. O. Roos, *J. Chem. Phys.* **74**, 2384 (1981).
- <sup>19</sup> K. Andersson, P.-Å. Malmqvist, B. O. Roos, A. J. Sadlej, and K. Wolinski, *J. Phys. Chem.* **94**, 5483 (1990).
- <sup>20</sup> K. Andersson, P.-Å. Malmqvist and B. O. Roos, *J. Chem. Phys.* **96**, 1218 (1992).
- <sup>21</sup> A. Zaitsevskii and J. P. Malrieu, *Chem. Phys. Lett.* **233**, 597 (1995).
- <sup>22</sup> J. Finley, P.-Å. Malmqvist, B. O. Roos and L. Serrano-Andrés, *Chem. Phys. Lett.* **288**, 299 (1998).
- <sup>23</sup> P. Ghigna, S. Pin, C. Ronda, A. Speghini, F. Piccinelli, and M. Bettinelli, *Opt. Mater.* **34**, 19 (2011).
- <sup>24</sup> P. A. Tanner, L. Fu, L. Ning, B.-M. Cheng, and M. G. Brik, *J. Phys.: Condens. Matter* **19**, 216213 (2007).
- <sup>25</sup> P. Hohenberg and W. Kohn, *Phys. Rev. B* **136**, B864 (1964).
- <sup>26</sup> W. Kohn and L. J. Sham, *Phys. Rev.* **140**, A1133 (1965).

- <sup>27</sup> G. Blasse and A. Bril, *J. Chem. Phys.* **47**, 5139 (1967).
- <sup>28</sup> T. Y. Tien, E. F. Gibbons, R. G. DeLosh, P. J. Zacmanidis, D. E. Smith, and H. L. Stadler, *J. Electrochem. Soc.* **120**, 278 (1973).
- <sup>29</sup> J. Dong and K. Lu, *Phys. Rev. B* **43**, 8808 (1991).
- <sup>30</sup> F. A. Selim, D. Solodovnikov, M. H. Weber, and K. G. Lynn, *Appl. Phys. Lett.* **91**, 104105 (2007).
- <sup>31</sup> A. B. Muñoz-García, E. Artacho, and L. Seijo, *Phys. Rev. B* **80**, 014105 (2009).
- <sup>32</sup> P. Ordejón, E. Artacho, and J. M. Soler, *Phys. Rev. B* **53**, R10441 (1996).
- <sup>33</sup> J. M. Soler, E. Artacho, J. D. Gale, A. García, J. Junquera, P. Ordejón, and D. Sánchez-Portal, *J. Phys.: Condens. Matter* **14**, 2745 (2002).
- <sup>34</sup> J. P. Perdew, K. Burke, and M. Ernzerhof, *Phys. Rev. Lett.* **77**, 3865 (1996).
- <sup>35</sup> J. P. Perdew, K. Burke, and M. Ernzerhof, *Phys. Rev. Lett.* **78**, 1396 (1997).
- <sup>36</sup> N. Troullier and J. L. Martins, *Phys. Rev. B* **43**, 1993 (1991).
- <sup>37</sup> L. Kleinman and D. M. Bylander, *Phys. Rev. Lett.* **48**, 1425 (1982).
- <sup>38</sup> A. B. Muñoz-García, E. Anglada, and L. Seijo, *Int. J. Quantum Chem.* **109**, 1991 (2009).
- <sup>39</sup> G. B. Bachelet, D. R. Hamann, and M. Schlüter, *Phys. Rev. B* **26**, 4199 (1982).
- <sup>40</sup> S. G. Louie, S. Froyen, and M. L. Cohen, *Phys. Rev. B* **26**, 1738 (1982).
- <sup>41</sup> E. Anglada, J. M. Soler, J. Junquera, and E. Artacho, *Phys. Rev. B* **66**, 205101 (2002).
- <sup>42</sup> F. Euler and J. A. Bruce, *Acta Crystallogr.* **19**, 971 (1965).
- <sup>43</sup> Z. Barandiarán and L. Seijo, *J. Chem. Phys.* **89**, 5739 (1988).
- <sup>44</sup> A. B. Muñoz-García and L. Seijo, *J. Phys. Chem. A* **115**, 815 (2011).
- <sup>45</sup> J. L. Pascual, N. Barros, Z. Barandiarán, and L. Seijo, *J. Phys. Chem. A* **113**, 12454 (2009).
- <sup>46</sup> L. Seijo, Z. Barandiarán, and B. Ordejón, *Mol. Phys.* **101**, 73 (2003).
- <sup>47</sup> S. Huzinaga, L. Seijo, Z. Barandiarán, and M. Klobukowski, *J. Chem. Phys.* **86**, 2132 (1987).
- <sup>48</sup> T. H. Dunning and P. J. Hay, in *Modern Theoretical Chemistry*, edited by H. F. Schaefer III (Plenum, New York, 1977).
- <sup>49</sup> J. Andzelm, M. Klobukowski, E. Radzio-Andzelm, Y. Sakai, and H. Tatewaki, *Gaussian Basis Sets for Molecular Calculations*, edited by S. Huzinaga, (Elsevier, Amsterdam, 1984).
- <sup>50</sup> Detailed core and embedding AIMP data libraries in electronic format are available from the authors upon request or directly at the address <http://www.uam.es/quimica/aimp/Data/-AIMPLibs.html>. See also Ref. 51.



- <sup>51</sup> G. Karlström, R. Lindh, P. A. Malmqvist, B. O. Roos, U. Ryde, V. Veryazov, P. O. Widmark, M. Cossi, B. Schimmelpfennig, P. Neogady, and L. Seijo, *Comput. Mater. Sci.* **28**, 222 (2003).
- <sup>52</sup> B. R. Judd, *Phys. Rev. Lett.* **39**, 242 (1977).
- <sup>53</sup> C. A. Morrison, *J. Chem. Phys.* **72**, 1001 (1980).
- <sup>54</sup> P. Dorenbos, *J. Lumin.* **87-89**, 970 (2000).
- <sup>55</sup> M. Bettinelli and R. Moncorgé, *J. Lumin.* **92**, 287 (2001).
- <sup>56</sup> Z. Barandiarán, N. M. Edelstein, B. Ordejón, F. Ruipérez, and L. Seijo, *J. Solid State Chem.* **178**, 464 (2005).

TABLE I: Off-center displacements of the substitutional atoms Ce<sub>Y</sub>, Y<sub>Al</sub>, and Al<sub>Y</sub> in Ce<sub>1</sub>AD:YAG with respect to the original sites in YAG, d<sub>off</sub>(Ce<sub>Y</sub>), d<sub>off</sub>(Y<sub>Al</sub>), and d<sub>off</sub>(Al<sub>Y</sub>); differences with off-center displacements in 1AD:YAG are shown in parentheses. Intercationic distances in YAG, Ce:YAG, and Ce<sub>1</sub>AD:YAG (differences with Ce:YAG in parentheses). Relative defect energies with respect to the most stable one,  $\Delta E$ . Distances in Å. Energies in meV and kJ/mol (in parentheses). All defects are labeled according to Fig.2 . Data for YAG and Ce:YAG are taken from Refs. 38 and 15 respectively.

defect	Ce <sub>1</sub> AD:YAG			YAG		Ce:YAG		Ce <sub>1</sub> AD:YAG		$\Delta E$
	d <sub>off</sub> (Ce <sub>Y</sub> )	d <sub>off</sub> (Y <sub>Al</sub> )	d <sub>off</sub> (Al <sub>Y</sub> )	d(Y-Al <sub>oct</sub> )	d(Y-Y)	d(Ce <sub>Y</sub> -Al <sub>oct</sub> )	d(Ce <sub>Y</sub> -Y)	d(Ce <sub>Y</sub> -Y <sub>Al</sub> )	d(Ce <sub>Y</sub> -Al <sub>Y</sub> )	
1a	0.013	0.134 (+0.004)	0.596 (-0.002)	5.459	6.057	5.458	6.060	5.473 (+0.015)	6.083 <sup>a</sup> (+0.023)	0 (0)
1b	0.070	0.135 (+0.005)	0.607 (+0.009)	5.459	3.709	5.458	3.718	5.285 (-0.173)	3.898 (+0.180)	154 (14.9)
1c	0.004	0.129 (-0.001)	0.592 (-0.006)	8.155	6.772	8.153	6.773	8.037 <sup>a</sup> (-0.116)	6.401 (-0.372)	163 (15.7)
1d	0.010	0.125 (-0.005)	0.581 (-0.017)	5.459	6.772	5.458	6.773	5.463 (+0.005)	6.450 <sup>a</sup> (-0.323)	180 (17.4)
1e	0.010	0.124 (-0.006)	0.583 (-0.015)	3.386	3.709	3.395	3.718	3.429 (+0.034)	3.818 (+0.100)	185 (17.8)
1f	0.009	0.122 (-0.008)	0.601 (+0.003)	8.155	7.103	8.153	7.106	8.151 (-0.002)	7.075 <sup>a</sup> (-0.031)	196 (18.9)
1g	0.119	0.140 (+0.010)	0.565 (-0.033)	3.386	3.709	3.395	3.718	3.428 (+0.033)	3.833 (+0.115)	200 (19.3)
1h	0.042	0.134 (+0.004)	0.599 (+0.001)	6.938	5.666	6.944	5.668	6.855 (-0.089)	6.064 (+0.396)	202 (19.5)
1i	0.003	0.126 (-0.004)	0.586 (-0.012)	5.459	5.666	5.458	5.668	5.381 (-0.077)	6.232 (+0.564)	208 (20.1)
1j	0.052	0.122 (-0.008)	0.569 (-0.029)	6.938	3.709	6.944	3.718	6.771 (-0.223)	3.628 (-0.090)	210 (20.3)
1k	0.013	0.134 (+0.004)	0.590 (-0.008)	8.155	7.103	8.153	7.106	8.052 (-0.101)	7.219 (+0.113)	215 (20.7)
1l	0.014	0.114 (-0.016)	0.582 (-0.016)	5.459	8.566	5.458	8.564	5.138 <sup>a</sup> (-0.320)	8.482 (-0.082)	285 (27.5)
1m	0.023	0.131 (+0.001)	0.584 (-0.014)	6.938	5.666	6.944	5.668	6.905 (-0.039)	5.381 (-0.287)	295 (28.5)
1n	0.076	0.132 (+0.002)	0.583 (-0.015)	3.386	6.772	3.395	6.773	3.651 (+0.256)	7.189 (+0.416)	303 (29.2)
1o	0.023	0.130 (0.000)	0.579 (-0.019)	6.938	6.772	6.944	6.773	6.861 <sup>a</sup> (-0.083)	6.395 (-0.378)	311 (30.0)
1p	0.083	0.119 (-0.011)	0.590 (-0.008)	3.386	5.666	3.395	5.668	3.485 (+0.090)	5.591 (-0.077)	351 (33.9)
1q	0.087	0.120 (-0.010)	0.591 (-0.007)	3.386	5.666	3.395	5.668	3.485 (+0.090)	6.285 (+0.617)	359 (34.6)
1r	0.041	0.132 (+0.002)	0.592 (-0.006)	6.938	7.103	6.944	7.106	6.935 (-0.009)	7.171 (+0.065)	403 (38.9)
1s	0.018	0.119 (-0.011)	0.591 (-0.007)	5.459	7.103	5.458	7.106	5.538 (+0.080)	6.989 (-0.117)	405 (39.1)
1t	0.021	0.130 (0.000)	0.590 (-0.008)	8.155	5.666	8.153	5.668	8.077 (-0.076)	5.378 (-0.290)	432 (41.7)
1u	0.021	0.132 (+0.002)	0.589 (-0.009)	6.938	8.566	6.944	8.564	6.928 <sup>a</sup> (-0.600)	7.964 <sup>a</sup> (-0.016)	436 (42.1)
1v	0.022	0.131 (+0.001)	0.584 (-0.014)	8.155	5.666	8.153	5.668	8.089 (-0.064)	5.378 (-0.290)	438 (42.3)
1w	0.029	0.128 (-0.002)	0.569 (-0.029)	8.155	10.491	8.153	10.493	8.156 <sup>a</sup> (+0.003)	10.440 (-0.053)	478 (46.1)

<sup>a</sup>Atoms located in adjacent unit cells.

TABLE II: Off-center displacements of  $\text{Ce}_Y$  in  $\text{Ce}_2\text{AD}:\text{YAG}$  with respect to its original site in YAG,  $d_{\text{off}}(\text{Ce}_Y)$ . Intercationic distances in YAG,  $\text{Ce}:\text{YAG}$ , and  $\text{Ce}_2\text{AD}:\text{YAG}$  (differences with  $\text{Ce}:\text{YAG}$  in parentheses).  $\text{Al}_{\text{oct}}$  is the Al atom of the most stable  $2\text{AD}:\text{YAG}$  structure that occupies an inversion center (Ref. 31). Relative defect energies with respect to the most stable one,  $\Delta E$ . Distances in Å. Energies in meV and kJ/mol (in parentheses). All defects are labeled according to Fig.2. Data for YAG and  $\text{Ce}:\text{YAG}$  are taken from Refs. 38 and 15 respectively.

defect	$\text{Ce}_2\text{AD}:\text{YAG}$ $d_{\text{off}}(\text{Ce}_Y)$	YAG $d(\text{Y}-\text{Al}_{\text{oct}})$	$\text{Ce}:\text{YAG}$ $d(\text{Ce}-\text{Al}_{\text{oct}})$	$\text{Ce}_2\text{AD}:\text{YAG}$ $d(\text{Ce}-\text{Al}_{\text{oct}})$	$\Delta E$
2k	0.039	8.155	8.153	8.133 (−0.020)	0 (0)
2f	0.077	8.155	8.153	8.107 (−0.046)	38 (3.7)
2w	0.086	8.155	8.153	8.134 (−0.019)	41 (4.0)
2h	0.075	6.938	6.944	6.870 <sup>a</sup> (−0.074)	55 (5.3)
2Al	0.083	3.386	3.395	3.378 (−0.017)	57 (5.5)
2a	0.050	5.459	5.458	5.414 (−0.044)	71 (6.9)
2u	0.031	6.938	6.944	6.910 <sup>a</sup> (−0.034)	89 (8.6)
2i	0.026	5.459	5.458	5.469 (+0.011)	115 (11.1)
2l	0.025	5.459	5.458	5.477 (+0.019)	118 (11.4)
2m	0.019	6.938	6.944	6.938 <sup>a</sup> (−0.006)	135 (13.0)
2a	0.115	3.386	3.395	3.332 (−0.063)	256 (24.7)

<sup>a</sup>Atoms located in adjacent unit cells.

TABLE III:  $\text{Ce}_Y\text{-O}$ ,  $\text{Al}_Y\text{-O}$ , and  $\text{Y}_{\text{Al}}\text{-O}$  distances (in Å) of the most stable  $\text{Ce,1AD:YAG}$  defect (defect 1a in Table. I; see Fig.3).

Oxygen	$d(\text{Ce}_Y\text{-O})^a$	Oxygen	$d(\text{Al}_Y\text{-O})^b$	Oxygen	$d(\text{Y}_{\text{Al}}\text{-O})^b$
s1	2.427 (+0.054)	d1	3.206 (−0.010)	b1	2.126 (−0.002)
s2	2.420 (+0.047)	d2	2.309 (−0.005)	b2	2.209 (−0.002)
s3	2.405 (+0.032)	d3	2.129 (−0.060)	o1	2.238 (+0.005)
s4	2.414 (+0.041)	d4	2.011 (−0.047)	o2	2.221 (−0.005)
l1	2.516 (+0.048)	d5	1.983 (+0.019)	o3	2.224 (+0.001)
l2	2.518 (+0.050)	d6	1.955 (+0.001)	o4	2.187 (+0.001)
l3	2.516 (+0.048)	b1	2.904 (+0.015)		
l4	2.450 (−0.018)	b2	2.019 (−0.045)		

<sup>a</sup>In parenthesis, differences with respect to  $\text{Ce:YAG}$  (Ref. 44).

<sup>b</sup>In parenthesis, differences with respect to  $\text{1AD:YAG}$  (Ref. 31).

TABLE IV:  $\text{Ce}_Y\text{-O}$ ,  $\text{Al}_Y\text{-O}$ , and  $\text{Y}_{\text{Al}}\text{-O}$  distances (in Å) of the most stable  $\text{Ce}_2\text{AD}:\text{YAG}$  defect (defect 2k in Table. I; see Fig.4).

Oxygen	$d(\text{Ce}_Y\text{-O})^a$	Oxygen	$d(\text{Al}_Y\text{-O})$	$d(\text{Al}_Y'\text{-O})^b$	Oxygen	$d(\text{Y}_{\text{Al}}\text{-O})$	$d(\text{Y}_{\text{Al}}'\text{-O})^b$
s1	2.376 (+0.003)	d1	3.338 (0.000)	3.263 (−0.075)	b1	2.123 (0.000)	2.116 (−0.007)
s2	2.419 (+0.046)	d2	2.100 (0.000)	2.096 (−0.004)	b2	2.212 (0.000)	2.203 (−0.009)
s3	2.402 (+0.029)	d3	2.169 (0.000)	2.154 (−0.015)	o1	2.216 (0.000)	2.236 (+0.020)
s4	2.447 (+0.074)	d4	2.056 (0.000)	2.033 (−0.023)	o2	2.226 (0.000)	2.225 (−0.001)
l1	2.492 (+0.024)	d5	2.080 (0.000)	2.098 (+0.018)	o3	2.224 (0.000)	2.228 (+0.004)
l2	2.498 (+0.030)	d6	1.966 (0.000)	1.959 (−0.007)	o4	2.190 (0.000)	2.187 (−0.003)
l3	2.504 (+0.036)	b1	2.854 (0.000)	2.854 ( 0.000)			
l4	2.553 (+0.085)	b2	2.057 (0.000)	2.063 (+0.006)			

<sup>a</sup>In parenthesis, differences with respect to  $\text{Ce}:\text{YAG}$  (Ref. 44).

<sup>b</sup>In parenthesis, differences with respect to  $2\text{AD}:\text{YAG}$  (Ref. 31).

TABLE V: Relative energies of the Ce- $4f^1$ , Ce- $5d^1$ , and Ce- $6s^1$  levels of Ce:YAG, Ce,1AD:YAG and Ce,2AD:YAG and their shifts induced by the presence of one and two antisite defects per unit cell, as a result of CASPT2 calculations on  $(\text{CeO}_8\text{Al}_2\text{O}_4)^{15-}$  embedded clusters. All numbers in  $\text{cm}^{-1}$ .

Material:		Ce:YAG <sup>a</sup>		Ce,1AD:YAG		Ce,2AD:YAG	
	$D_2$	Energy	$C_1$	Energy	Shift	Energy	Shift
$4f^1$ levels							
	$1\ ^2B_2$	0	$1\ ^2A$	0	0	0	0
	$1\ ^2B_3$	38	$2\ ^2A$	63	26	36	-1
	$1\ ^2B_1$	202	$3\ ^2A$	159	-43	271	69
	$1\ ^2A$	416	$4\ ^2A$	433	17	461	45
	$2\ ^2B_1$	443	$5\ ^2A$	488	45	492	49
	$2\ ^2B_2$	516	$6\ ^2A$	571	55	624	108
	$2\ ^2B_3$	2419	$7\ ^2A$	2316	-102	2320	-98
$5d^1$ levels							
	$2\ ^2A$	23853	$8\ ^2A$	24314	461	24645	792
	$3\ ^2B_3$	30169	$9\ ^2A$	31093	923	30505	336
	$3\ ^2A$	48112	$10\ ^2A$	47904	-208	46695	-1418
	$3\ ^2B_2$	48700	$11\ ^2A$	49318	618	47379	-1321
	$3\ ^2B_1$	52221	$12\ ^2A$	50218	-2003	52497	276
$6s^1$ level							
	$4\ ^2A$	61214	$13\ ^2A$	58984	-2230	64190	2976

<sup>a</sup>Reference 15.

TABLE VI:  $4f^1$ ,  $5d^1$ , and  $6s^1$  levels of the  $(\text{CeO}_8\text{Al}_2\text{O}_4)^{15-}$  cluster in several embedding potentials.

Calculation	Ce:YAG $A^a$	B	Ce,1AD:YAG C	D	B	Ce,2AD:YAG C	D
Cluster coordinates	Ce:YAG	Ce,1AD:YAG	Ce,1AD:YAG	Ce,1AD:YAG	Ce,2AD:YAG	Ce,2AD:YAG	Ce,2AD:YAG
Embedding coordinates	Ce:YAG	Ce:YAG	Ce,1AD:YAG	Ce,1AD:YAG	Ce:YAG	Ce,2AD:YAG	Ce,2AD:YAG
Embedding potential on $\text{Al}_Y\text{-Y}_{\text{Al}}$	$\text{Y}_Y\text{-Al}_{\text{Al}}$	$\text{Y}_Y\text{-Al}_{\text{Al}}$	$\text{Y}_Y\text{-Al}_{\text{Al}}$	$\text{Al}_Y\text{-Y}_{\text{Al}}$	$\text{Y}_Y\text{-Al}_{\text{Al}}$	$\text{Y}_Y\text{-Al}_{\text{Al}}$	$\text{Al}_Y\text{-Y}_{\text{Al}}$
$1^2A$	0	0	0	0	0	0	0
$2^2A$	38	112	85	63	55	38	36
$3^2A$	202	142	152	159	265	223	271
$4^2A$	416	460	441	433	489	401	461
$5^2A$	443	510	498	488	516	443	492
$6^2A$	516	601	587	571	639	559	624
$7^2A$	2419	2354	2324	2316	2355	2271	2320
$8^2A$	23853	24094	24288	24314	24336	24887	24645
$9^2A$	30169	31007	31135	31093	30703	30614	30505
$10^2A$	48112	47760	47820	47904	47077	46703	46695
$11^2A$	48700	49240	49294	49318	47510	47473	47379
$12^2A$	52221	51476	50296	50218	52517	52254	52497
$13^2A$	61214	61311	60472	58984	63873	60256	64190
$\Delta E_{\text{centroid}}(4f^1 \rightarrow 5d^1)$	40035	39919	39983	39994	39812	39824	39743
$\Delta E_{\text{LF}}(1-4f^1)$	576	597	584	576	617	562	601
$\Delta E_{\text{LF}}(1-5d^1)$	16758	16421	16279	16256	16093	15499	15699
$\Delta E_{\text{ligand-field}}(1-4f^1 \rightarrow 1-5d^1)$	-16182	-15824	-15695	-15680	-15476	-14937	-15098
$\Delta E_{\text{LF}}(2-5d^1)$	10442	9508	9432	9477	9725	9773	9839
$\Delta E_{\text{ligand-field}}(1-4f^1 \rightarrow 2-5d^1)$	-9866	-8911	-8848	-8901	-9109	-9210	-9238

<sup>a</sup>Reference 15.

TABLE VII: Analysis of contributions to the shift of the first  $4f \rightarrow 5d$  transition from Ce:YAG to Ce,1AD:YAG and Ce,2AD:YAG. All numbers in  $\text{cm}^{-1}$ .

	First-shell distortion	Contributions Full distortion	$\text{Al}_Y\text{-Y}_{\text{Al}}$	All
Ce,1AD:YAG				
$\Delta E_{\text{centroid}}(4f^1 \rightarrow 5d^1)$	-116	-52	11	-41
$\Delta E_{\text{LF}}(1 - 4f^1)$	21	8	-8	0
$\Delta E_{\text{LF}}(1 - 5d^1)$	-337	-479	-23	-502
$\Delta E_{\text{ligand-field}}$	357	487	15	502
$\Delta E$	241	435	26	461
Ce,2AD:YAG				
$\Delta E_{\text{centroid}}(4f^1 \rightarrow 5d^1)$	-223	-211	-81	-292
$\Delta E_{\text{LF}}(1 - 4f^1)$	41	-14	39	25
$\Delta E_{\text{LF}}(1 - 5d^1)$	-665	-1259	200	-1059
$\Delta E_{\text{ligand-field}}$	706	1245	-161	1084
$\Delta E$	483	1034	-242	792



FIG. 1: Representation of the  $(\text{CeO}_8\text{Al}_2\text{O}_4)^{15-}$  embedded cluster used in this work.

FIG. 2: Non-equivalent sites of the  $\text{Ce}_Y$  substitutional defect in the YAG unit cell with respect to the most stable single (top) and double (bottom)  $\text{Al}_Y\text{-Y}_{\text{Al}}$  antisite defects. The most stable locations for  $\text{Ce}_Y$  in each case are underlined.

FIG. 3: Most stable  $\text{Ce}_Y\text{-1AD}$  defect (1a in Fig. 2). Detailed structure (top) and axial periodicity showing the  $\dots\text{-Ce}_Y\text{-AlO}_4\text{-Al}_Y\text{-AlO}_4\text{-Ce}_Y\text{-}\dots$  chain (bottom).

FIG. 4: Most stable  $\text{Ce}_Y\text{-2AD}$  defect (2k in Fig. 2).

FIG. 5: Schematic representation of defect formation energies. All energies in eV.

FIG. 6: DOS and PDOS of  $\text{Ce}_Y\text{-1AD:YAG}$  (defect 1a): Orbital decomposition of the Ce  $\alpha$  PDOS, PDOS of Ce, Y, Al and O atoms, and total DOS.

FIG. 7: DOS and PDOS of  $\text{Ce}_Y\text{-2AD:YAG}$  (defect 2k): Orbital decomposition of the Ce  $\alpha$  PDOS, PDOS of Ce, Y, Al and O atoms, and total DOS.

FIG. 8: Ce  $\alpha$  PDOS around the band gap in  $\text{Ce:YAG}$  (Ref. 15),  $\text{Ce}_Y\text{-1AD:YAG}$  (defect 1a) and  $\text{Ce}_Y\text{-2AD:YAG}$  (defect 2k).

FIG. 9: Schematic representation of the  $4f^1$  and  $5d^1$  manifolds of the  $\text{Ce}_Y$  defect.

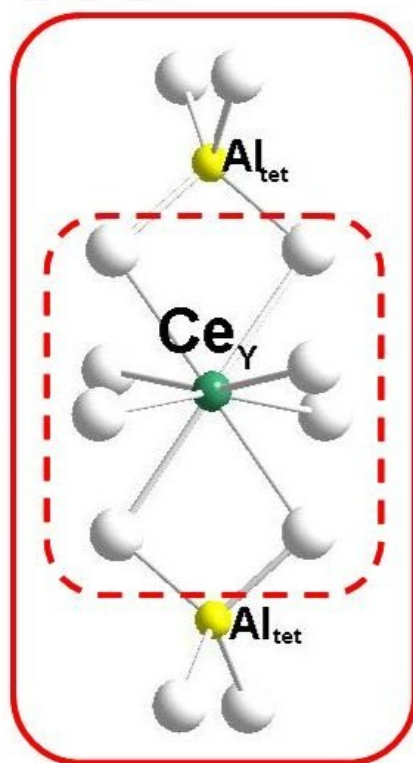


Figure 1 Muñoz-García *et al.*

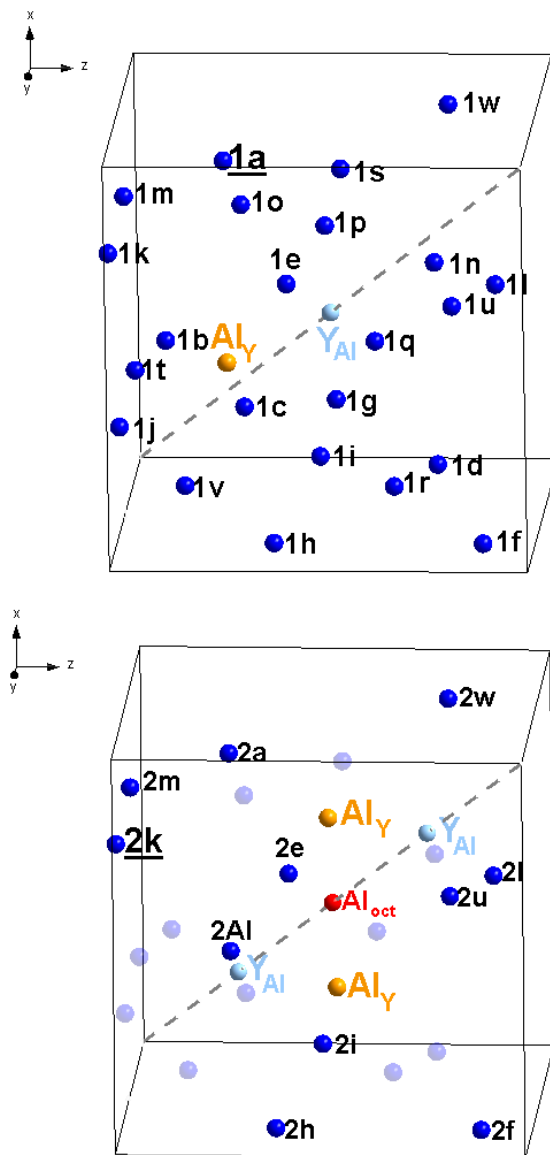


Figure 2 Muñoz-García *et al.*

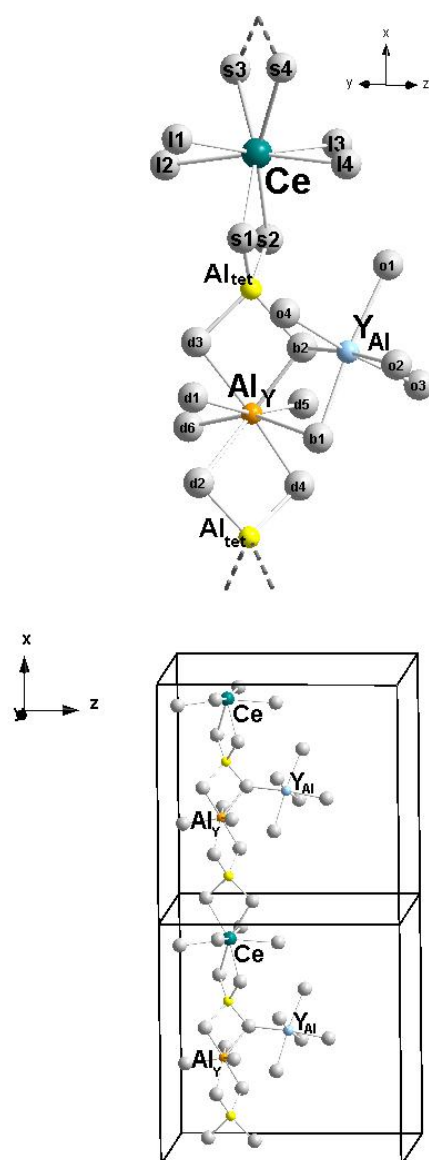


Figure 3 Muñoz-García *et al.*

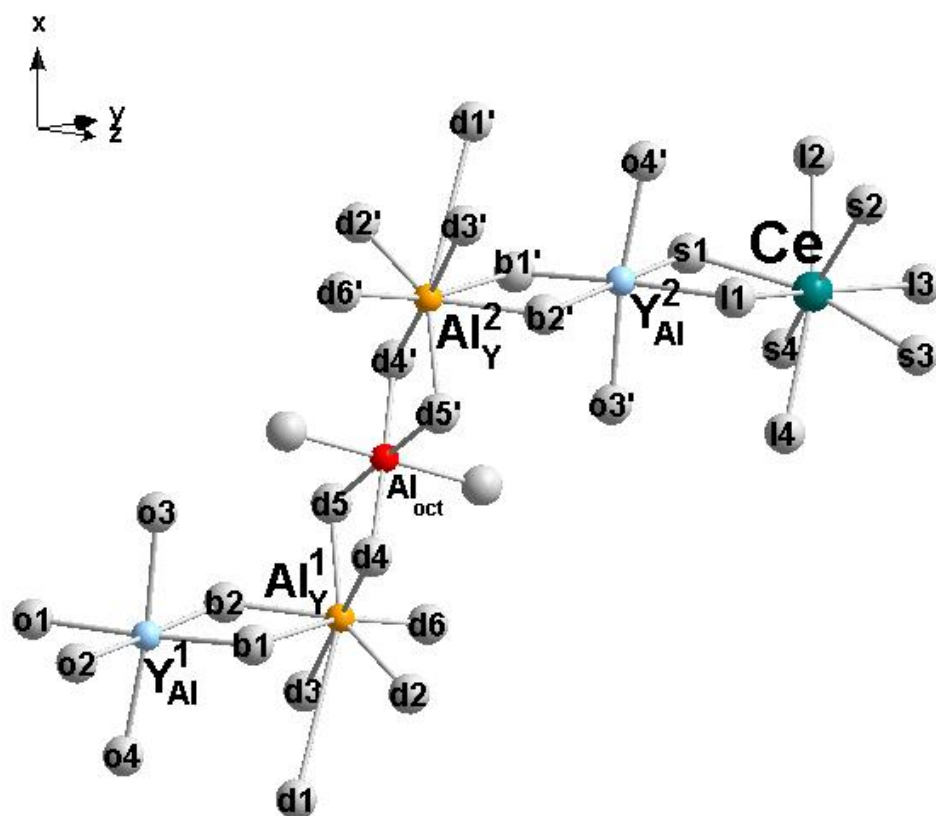


Figure 4 Muñoz-García *et al.*

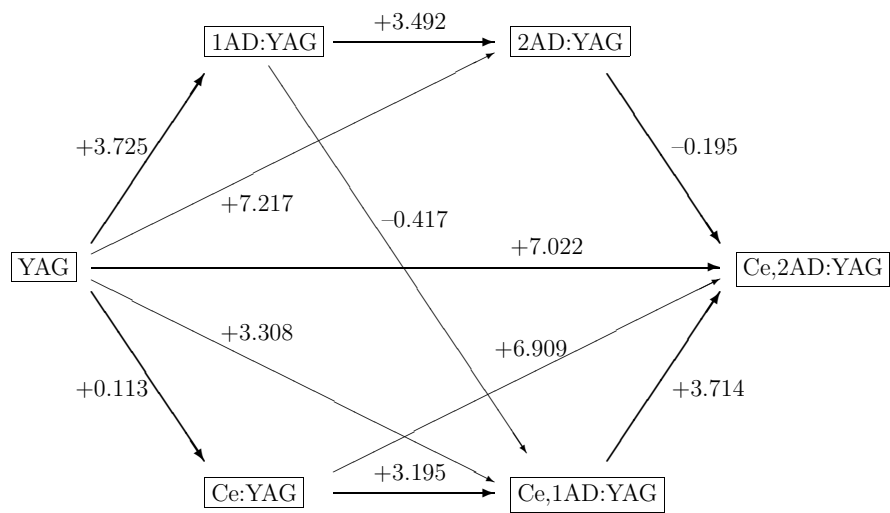


Figure 5 Muñoz-García *et al.*

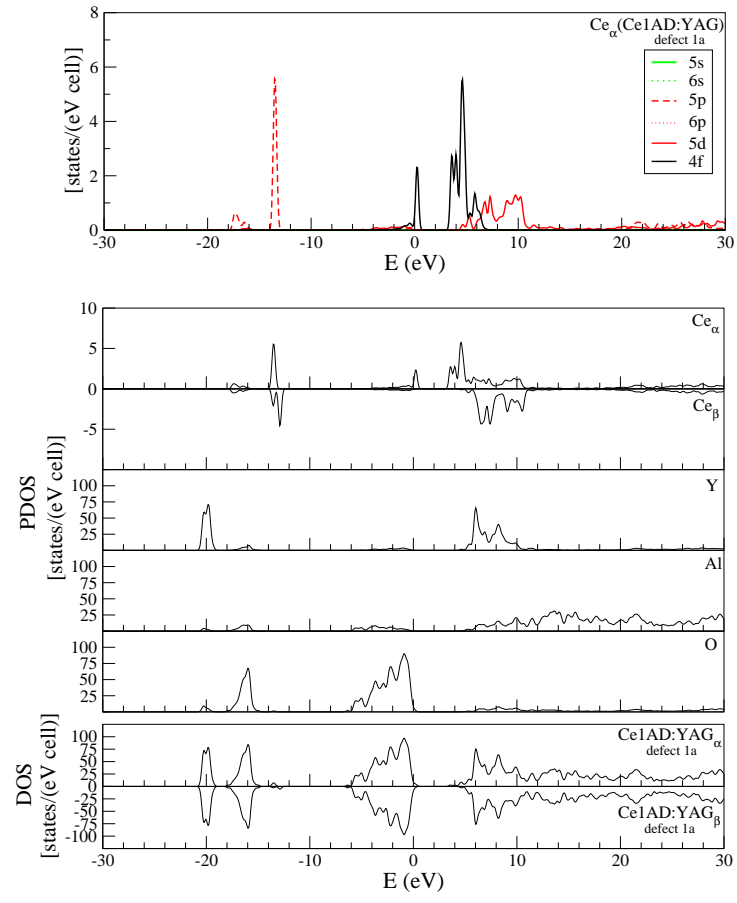


Figure 6 Muñoz-García *et al.*

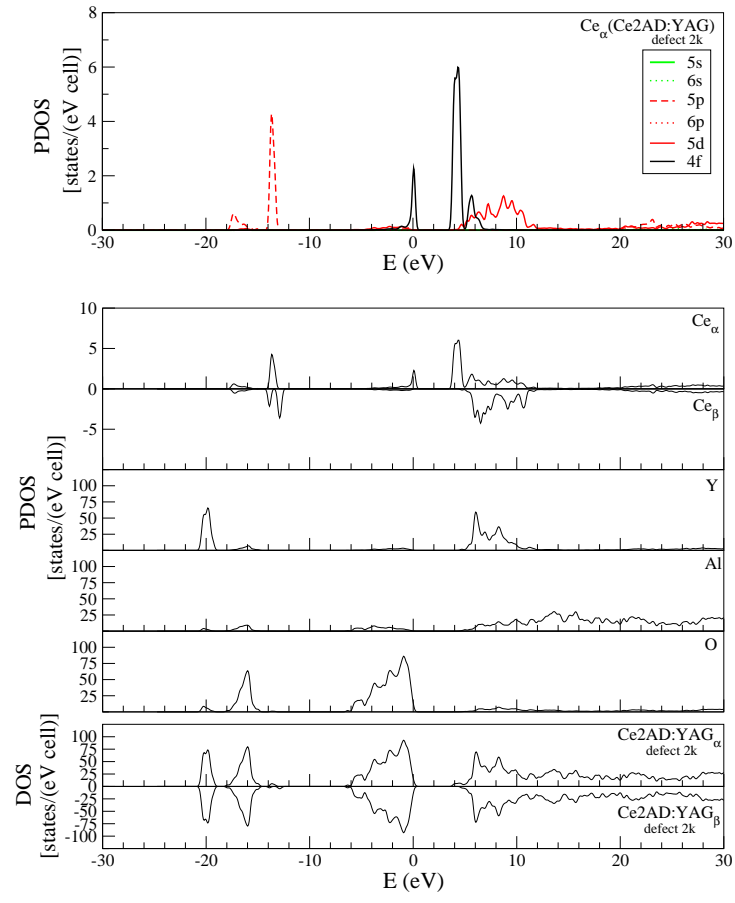


Figure 7 Muñoz-García *et al.*



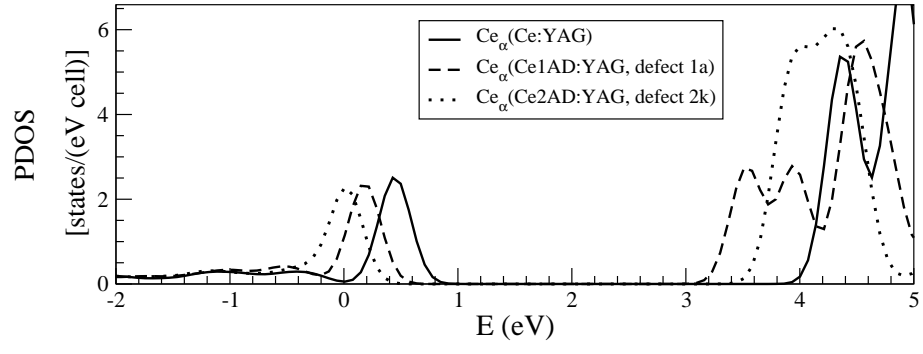


Figure 8 Muñoz-García *et al.*

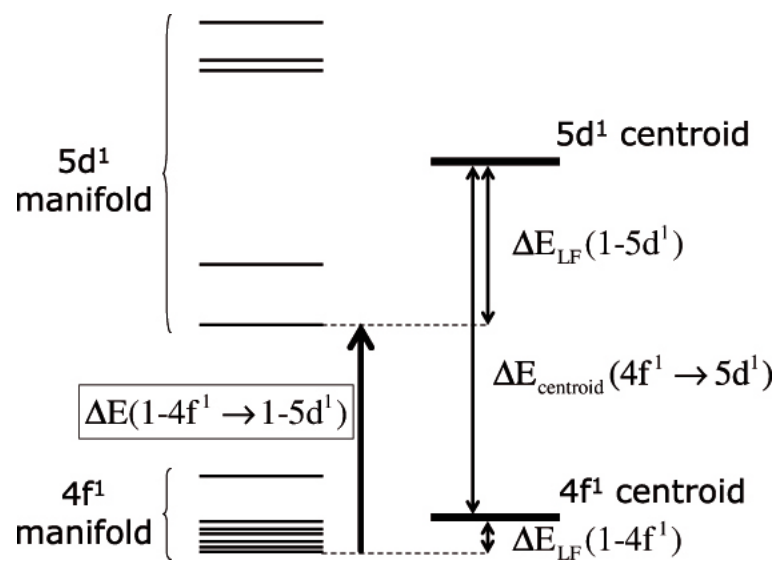


Figure 9 Muñoz-García *et al.*